Published as: *Cell*. 2008 May 16; 133(4): 585–600.

SMN deficiency causes tissue-specific perturbations in the repertoire of snRNAs and widespread defects in splicing

Zhenxi Zhang[1], **Francesco Lotti**[1], **Kimberly Dittmar**, **Ihab Younis**, **Lili Wan**, **Mumtaz Kasim**, and **Gideon Dreyfuss**[*]
Howard Hughes Medical Institute, Department of Biochemistry and Biophysics, University of Pennsylvania School of Medicine, Philadelphia, Pennsylvania 19104-6148

Summary

The survival of motor neurons protein (SMN) is essential for the biogenesis of small nuclear RNA (snRNA)-ribonucleoproteins (snRNPs), the major components of the pre-mRNA splicing machinery. Though it is ubiquitously expressed, SMN deficiency causes the most common motor neuron degenerative disease, spinal muscular atrophy (SMA). We show here that SMN deficiency, similar to that which occurs in severe SMA, has unexpected cell type-specific effects on the repertoire of snRNAs and mRNAs. It alters the stoichiometry of snRNAs and causes widespread pre-mRNA splicing defects in numerous transcripts of diverse genes, preferentially those containing a large number of introns, in SMN-deficient mouse tissues. These findings reveal a key role for the SMN complex in RNA metabolism and in splicing regulation, and indicate that SMA is a general splicing disease that is not restricted to motor neurons.

Introduction

The survival of motor neurons (SMN) protein is part of a large multi-protein complex (the SMN complex) that also contains at least seven additional proteins, termed Gemins 2–8 (Baccon et al., 2002; Carissimi et al., 2006; Charroux et al., 1999; Charroux et al., 2000; Gubitz et al., 2002; Liu et al., 1997; Pellizzoni et al., 2002a). The SMN complex is an assemblyosome that is essential for the biogenesis of small nuclear ribonucleoprotein particles (snRNPs) (Fischer et al., 1997; Meister et al., 2001; Pellizzoni et al., 2002b; Yong et al., 2004). snRNPs are major components of the spliceosome, the machinery that carries out pre-mRNA splicing (Nilsen, 2003; Will and Luhrmann, 2001). Each of the spliceosomal snRNPs (except for U6 and U6atac) is comprised of one snRNA (U1, U2, U4, U5, U11, U12, and U4atac) and a set of seven common proteins called the Sm proteins, as well as one or more proteins that are specific to each snRNA (Kambach et al., 1999; Nilsen, 2003; Will and Luhrmann, 2001). The assembly of heptameric Sm protein rings on snRNAs (Sm cores) is strictly dependent on the SMN complex (Meister et al., 2001; Pellizzoni et al., 2002b; Wan et al., 2005).

Genetic lesions in the SMN gene (*SMN1*) that result in functional SMN protein deficiency are the cause of spinal muscular atrophy (SMA) (Lefebvre et al., 1995), the most common motor neuron degenerative disease and the leading genetic cause of infant mortality (Cifuentes-Diaz et al., 2002; Iannaccone et al., 2004; Talbot and Davies, 2001). A second copy of the gene, *SMN2*, contains a single nucleotide mutation in exon 7 which results in frequent skipping of

* Corresponding author: gdreyfuss@hhmi.upenn.edu.
[1]These authors contributed equally to this work

this exon and, consequently, low levels of functional SMN protein (Lorson et al., 1999). Although SMN is ubiquitously expressed in all tissues and is essential for viability of all cells in diverse eukaryotic organisms (Paushkin et al., 2002; Schrank et al., 1997; Wang and Dreyfuss, 2001), the question of how reduction in SMN levels results in an apparently cell-selective motor neuron phenotype remains unexplained (Monani, 2005). The SMN-dependent Sm core assembly reaction can be studied in cell extracts, and the amount of Sm core assembly on the snRNAs corresponds directly to the amount of SMN protein and can be modulated by the other components of the SMN complex (Battle et al., 2006b; Feng et al., 2005; Wan et al., 2005). Indeed, extracts of SMA patient cells have a lower snRNP assembly capacity, corresponding to the lower amount of SMN protein they contain (Wan et al., 2005). These and other findings indicate that the deficiency in the activity of the SMN complex in snRNP assembly is relevant to the pathogenesis of SMA (Winkler et al., 2005). Several other functions for the SMN complex in RNA metabolism have been suggested, including functions in transcription (Pellizzoni et al., 2001b), pre-mRNA splicing (Fischer et al., 1997; Pellizzoni et al., 1998), the biogenesis of small nucleolar RNPs (snoRNPs) (Charroux et al., 2000; Pellizzoni et al., 2001a; Whitehead et al., 2002), and in axonal RNA transport (Jablonka et al., 2004; Pagliardini et al., 2000; Rossoll et al., 2003; Zhang et al., 2003), but these remain uncharacterized.

The studies described here were initiated to determine what effect a deficiency in SMN, and hence in the capacity of cells to produce snRNPs, has on the steady-state levels of spliceosomal snRNPs. We quantitated snRNAs in cell lines with reductions in SMN levels and an SMA mouse model, an SMN-deficient organism. Unexpectedly, we found that SMN deficiency does not cause a uniform reduction in snRNPs but rather has cell type- and snRNA-specific effects, resulting in profoundly different repertoires of snRNPs compared to those that contain normal SMN levels. In light of the alterations in the normal repertoire of the major constituents of the splicing machinery, we used exon microarrays to examine in detail if any changes occurred in the splicing patterns in several tissues of SMA mice compared to their unaffected littermates. We show that splicing defects occur in numerous mRNAs in multiple tissues of SMA mice, and conclude that SMN plays a key general role in RNA processing. The observation that deficiency of the ubiquitously expressed SMN results in cell type-specific splicing defects provides a new perspective on SMA and a plausible explanation for the selectivity of SMA pathogenesis.

Results

Alterations in snRNA levels in SMN-deficient cells

To study the effect of reduced levels of SMN on the amount of snRNAs, we established an inducible RNAi system for regulated knockdown of SMN. Short hairpin RNAs (shRNAs) specifically targeting either the human or mouse SMN mRNAs under the transcriptional control of a tetracycline-inducible H1 promoter were constructed in a lentiviral vector (Figure 1A). The two vectors were packaged into viral particles and used first to transduce a HeLa cell line (T-REx) constitutively expressing the tetracycline repressor (TR) protein. In this case, the non-targeting mouse SMN shRNA was used as the control. Binding of doxycycline to the TR activates transcription of the shRNA, resulting in RNAi, and the extent of SMN reduction was depended on the multiplicity of infection and on doxycycline concentration, and was determined by quantitative Western blots. Reduction of SMN level to ~20% (Figure S1A) of control had no effect on cell growth rate or morphology (data not shown). SMN levels could be further reduced to ~5% of normal, and the cells survived under these conditions for an additional 2–3 days before cell death was evident (data not shown). The capacity of assembly of Sm cores on snRNAs was measured using a quantitative assay in cell extracts (Wan et al., 2005), and it corresponded directly to the amount of SMN protein (Figure S1A).

To determine the effect of the reduction in snRNP assembly capacity on the steady-state level of snRNAs, we carried out real-time RT-PCR measurements for each of the spliceosomal snRNAs. Despite the strong reduction (almost 80%) in snRNP assembly capacity, there was no significant change in snRNA levels (Figure S1B). A further reduction in SMN levels, to ~15% or less of normal levels, was necessary to observe significant changes in snRNA levels. Using Western blots, we measured the levels of all the major components of the SMN complex, including SMN, the Gemins, and Unrip, as well as α-tubulin and Magoh which served as loading controls (Figure 1B). In addition to the strong reduction in SMN, a severe reduction was observed also for Gemin8 (87% before and 94% after induction), Gemin2 (58% before and 86% after induction) and Gemin3 (67% before and 75% after induction). In contrast, Gemin5, Gemin4 and Unrip remained unchanged. The snRNP assembly activity in these cells was also strongly reduced in close correlation with the amount of SMN protein remaining in these cells after RNAi induction (data not shown).

As shown in Figure 1C, in the absence of doxycycline and with only ~15% of SMN remaining, a moderate reduction in U4, U5, U12 and U4atac snRNAs was observed. However, a more severe decrease in SMN, to ~5% of normal, resulted in a pronounced reduction, albeit to different extents, of most of the snRNAs except U2 and U6. A very similar profile was observed measuring the snRNAs in mature snRNPs obtained by immunoprecipitation with Y12, a monoclonal antibody against Sm proteins (Figure S2). This is consistent with previous reports that the pool of snRNAs outside of snRNPs is relatively very small, as snRNAs that are not assembled with Sm cores are unstable (Sauterer et al., 1988; Zieve et al., 1988). These observations suggest that HeLa cells have a large excess capacity to produce snRNPs over what they require for viability. Importantly, once the level of SMN drops below a critical threshold (~15–20% of normal in these cells), the cellular contents of snRNAs is altered, but the change is not uniform as different snRNAs are affected to different extents.

To determine if a similar change in snRNAs occurs upon SMN deficiency in other cell types and species, we carried out similar measurements in a mouse motor neuron-derived cell line (MN1). MN1 cells were transduced with lentivirus expressing either the shRNA targeting mSMN or the non-targeting hSMN as control. Measurements of the amount of each of the snRNAs in MN1 cells where SMN levels were reduced to less than 10% of normal (Figure S3A), showed a small increase in U1 snRNA (16%) and a large decrease in U11 snRNA (40%) compared to control (Figure S3B). Importantly, the change in the profile of snRNAs in MN1 and in HeLa cells with a similar degree of SMN deficiency were markedly different, indicating that SMN deficiency causes cell type-specific alterations in the repertoire of snRNAs.

A decrease in SMN complex proteins and snRNP assembly capacity in SMA mice

To assess whether the observations described above can be extended to the level of an organism and their potential relevance to SMA, we performed similar studies in tissues of SMN-deficient mice. For this, we used a moderate SMA mouse model corresponding to a type II SMA phenotype (Le et al., 2005), as the affected animals survive for up to 14 days after birth, which allows the collection of various tissues at different stages as the disease progresses. Here, we used both 6-day old mice, at which time the phenotype begins to become evident, and 11-day old mice representing an advanced stage of the disease. Tissues harvested from homozygous *mSmn*$^{-/-}$ SMA mouse littermates and their unaffected heterozygous littermates at 6 (P6) and 11 days (P11) after birth were used for preparation of whole tissue extracts for Western blot, measurement of snRNP assembly activity, and isolation of total RNA for quantitative RT-PCR.

As expected, the level of SMN was severely reduced to ~15% of control in both brain and kidney (Figure 2A). Consistent with observations in other SMN deficiency systems (Wang and Dreyfuss, 2001), Gemin2 also showed significant reduction in SMA mice (~55% in brain and ~48% in kidney), and Gemin8 was severely reduced to an extent similar to that of SMN in both

brain and kidney of SMA mice, indicating a key role for SMN in maintaining the stability of the entire SMN complex. The extent of reduction in the level of SMN and other SMN complex components was very similar between P6 and P11 mice (data not shown). snRNP assembly activity was measured in total tissue extracts from brain and kidney in P6 and from brain, kidney, spinal cord and heart in P11 control and SMA mice. Considerable levels of snRNP assembly activity were detected in tissue extracts from P6 mice, whereas extracts of tissues of P11 mice had extremely low levels of activity, in accordance with the previously reported down-regulation of SMN complex activity during mouse development (Gabanella et al., 2005). In close parallel to the reduction in SMN levels, snRNP assembly activity in SMA mice was reduced by 75–80% in brain and kidney of P6 mice compared to the unaffected controls (Figure 2B).

Tissue-specific alterations in snRNAs in SMA mice

Total RNA isolated from brain of P6 mice and from brain, spinal cord, kidney, heart and skeletal muscle of P11 mice was used for real-time RT-PCR measurements of snRNAs. Significant changes in the stoichiometry of snRNAs were already apparent in P6 SMA mice (Figure 3). Marked reductions in some of the minor spliceosomal snRNAs in P11 SMA mice were detected, including U11, U12 and U4atac, which were reduced by ~30% to ~60% in brain, spinal cord and heart compared to the corresponding unaffected controls (Figure 3). This reduction in the minor (U12-dependent) spliceosomal pathway snRNAs is tissue-specific, as the same snRNAs in kidney and skeletal muscle are relatively unaffected in the SMA mice (Figure 3). In addition, we note that the levels of some major spliceosomal snRNAs, particularly U6 snRNA in heart, U2 and U6 snRNAs in kidney, and U1, U2, U5 and U6 snRNAs in skeletal muscle of SMA mice, were significantly increased compared to those of control mice (Figure 3), while the levels of 5S and 5.8S rRNAs, which were used as input normalization controls, were not significantly changed (data not shown). Recently, after submission of this manuscript, Gabanella et al. have also reported a decrease in some of the minor snRNAs in SMA mouse tissues (Gabanella et al., 2007).

Similar results were obtained using limited primer extension, an alternative method for measuring the amounts of RNA, which also illustrated the very large difference in abundance of the major and minor spliceosomal snRNAs. Shown in Figure S4, the measurement of U1, U11, U12 and U4atac snRNAs from brains of P11 control and SMA mice indicated a 25–35% reduction in the levels of U11, U12 and U4atac snRNAs in SMA mice, while U1 snRNA remained unchanged, consistent with the real-time RT-PCR data described above.

Widespread splicing perturbations in tissues of SMN-deficient mice

Although the alterations in the normal repertoire of snRNAs in SMN-deficient cells and in SMA mouse tissues were remarkable, they did not appear to cause a catastrophic collapse of splicing because, except for motor neurons, there was no evidence of cell death. We therefore used the high resolution afforded by exon microarrays to ask if there are any changes in splicing in SMA compared to control mice. To do so, total RNA from three tissues, spinal cord, brain, and kidney of three SMA mice and three unaffected littermates, each prepared and processed separately, were analyzed using the Affymetrix mouse exon 1.0 ST microarray. Among the 266,200 probe sets supported by putative full-length mRNA, around 200,000 probe sets with significant signals above background and representing exons of ~20,000 out of ~30,000 genes in the mouse genome (Waterston et al., 2002) were included in the analysis. With a False Discovery Rate (FDR) set at less than 0.1, 259, 73, and 633 genes from spinal cord, brain, and kidney were identified having potential splicing pattern changes, respectively (Table S1). The top 30 affected genes from each tissue, ranked by absolute fold change of the most affected exon of each transcript, are listed in Table 1. A relatively small number of genes showed ≥ 1.5 fold change across all exons (42, 0, and 264 genes from spinal cord, brain, and kidney,

respectively), indicating a much higher prevalence of splicing changes compared to transcription changes (Table S2).

To assess the validity of the exon array data we performed real-time RT-PCR, on 31 genes (indicated by Q under Validation & Characterization in Table 1), using exon junction specific primers and total RNA from the same control and SMA mice used in the exon array. Except for one, where the signal with the selected primers was too low for definitive measurement, all confirmed the changes observed in the exon array, indicating a validation rate of 97%.

In addition to measuring the amount of the exon in the tissue from which the signal was originally selected for the purpose of validation of the exon array data, we also determined the expression levels of the same exon in several other tissues, including brain, spinal cord, muscle, heart, and kidney, in both the control and SMA mice (Figure 4). These comprehensive measurements were performed on eight of the genes listed in Table 1 (indicated by Q*), including three types of transporter proteins (Abca8a, Kcng4 and Slc38a5), an extracellular matrix protein (Col5a1), Uspl1, Agxt2l1, Hif3a, and Chodl. Importantly, these measurements revealed a wide variation in the levels of these exons in different tissues, indicating the alterations in splicing are tissue-specific.

Figure 5 presents a summary of the exon array data for seven of these genes and indicates several additional validation experiments performed in the control and SMA mice. The height of the bars indicates the fold change between SMA and control for the probe sets representing each of the exons. The signal intensity for each of these is shown in Figure S5. The small error bars reflect the low variability among the three control and the three SMA mice used in the exon array experiments. Importantly, these measurements indicated that both transcript- and tissue-specific alterations in splicing occurred upon SMN deficiency.

To further validate and characterize the specific changes in the transcripts, we performed high-throughput (HT) RT-PCR and analyzed the products by high resolution capillary electrophoresis (Klinck et al., 2008). This large-scale analysis, consisting of more than 4,000 RT-PCR reactions in pairs of control and SMA, surveyed 22 of the genes in Table 1 (indicated as R). All the data of these experiments, including the sequences and locations of primers used for the HT RT-PCR, the electrophoregrams, the sizes and molarities of the products, and their positions on the gene maps, are accessible online (see Experimental Procedures). Because of space limitations, only a few representative examples are presented here. The locations of specific changes observed in some of these genes are indicated in Figure 5 (brackets labeled by R), and electrophoregrams of four pairs of RT-PCR reactions are shown in Figure 6. These data revealed numerous perturbations in the normal transcriptome. At least 17 of the examined genes (77%) contained changes predicted by the exon array data, but a considerable number of additional changes were documented. In some cases, the changes could be explained as alternative splicing where the ratio of two spliced isoforms is altered, however many others suggest aberrant splicing with isoforms present in SMA mice that are not found in the unaffected control littermates, and often do not correspond to a previously reported spliced isoform, or are outright defective as they produce a transcript that does not conform to normal splicing sites.

Examples of some of the many striking cases of specific alternative splicing changes and aberrant splicing events detected in the SMA mice are presented in Figure 6. The electrophoregrams illustrate several types of transcript changes in different tissues of the SMA mice, including changes in relative amounts of two likely alternatively spliced exons (Agxt2l1 & Lrdd), changes in the amount of several exons in the same transcript (Abca8a), and an example of aberrant splicing (Hif3a). Another two cases of aberrant splicing events were shown in Figures 5 and S6, where aberrant splicing products were detected by RT-PCR, then

sequenced, and their amounts were measured by real-time RT-PCR in control and SMA mice. For Col5a1, the aberrant transcript, which was only detectable in the SMA mice, skipped the last 223 nt of exon 62 and first 21 nt of exon 63, creating premature termination codons (PTCs) in the new open reading frame (ORF) (Figures 5 and S6A). Similarly, an aberrant transcript from Uaca in which exon 3 is skipped and PTCs were generated in the ORF was detected in SMA mice (Figures 5 and S6B). The generation of PTCs explains why the relative amount of the aberrant transcripts is, in many cases, relatively low and difficult to detect. The reduction in the level of the normal transcript, for example, ~50% for Col5a1, is consistent with a scenario in which about half of the pre-mRNA is aberrantly spliced but only a fraction of that is detectable because it is eliminated by nonsense-mediated decay (NMD).

Functional annotations of the most affected genes in the three tissues using Database for Annotation, Visualization and Integrated Discovery (DAVID), indicated that a wide diversity of genes were affected and revealed an over-representation of genes expressing transporter and extracellular matrix proteins. The functional annotations of the 30 most highly affected genes for each of the tissues are listed in Table 1. Although the number of affected genes common to all three tissues is small (only 2 genes), transcripts of transporter and extracellular matrix genes are particularly affected in all three tissues. These classes of genes have particularly large numbers of exons. In fact, among the 259, 73, and 633 affected genes in SMA mice spinal cord, brain, and kidney, the median number of exons in the affected transcripts is 14, 10, and 12, respectively. In the mouse genome, the median number of exons per transcript is only 6 (Waterston et al., 2002). This suggests that pre-mRNAs with more introns (exons) to splice are more vulnerable to splicing changes in SMA mice.

Discussion

Our findings here demonstrate that SMN deficiency causes profound changes in cellular RNA metabolism. It alters the repertoire of snRNAs and perturbs pre-mRNA splicing, leading to numerous splicing defects. The defects are widespread and cell-type specific, affecting mRNAs of functionally diverse genes. These surprising discoveries place the SMN complex, the essential machinery for the biogenesis of snRNPs, as a major factor in splicing regulation. Furthermore, they provide an example of how a deficiency in a ubiquitous protein can result in tissue-specific changes, and cast a new light on the pathophysiology of SMA.

A large degree of SMN decrease (> 80%) is required to cause a significant change in the levels of snRNAs, or cause cell death in cultured cells, suggesting that cells normally contain a large excess capacity of SMN complex to maintain their normal inventory of snRNAs. While a reduction in the amount of snRNAs upon decrease in SMN was not unexpected, its non-uniformity across different snRNAs and its cell type-specificity were unanticipated. Immunoprecipitation of snRNPs from total extract, which could be reliably performed from tissue cultured cells but not from mouse tissues, showed a similar stoichiometry for snRNAs in total RNA preparations and in snRNPs, consistent with previous observations that the pool of unassembled snRNAs is very small, and suggest that the cells have a similarly altered repertoire of snRNPs. The biogenesis of snRNPs is a highly regulated and intricate stepwise process, and the SMN complex is essential for the key step of the Sm core assembly on which all subsequent steps depend (Battle et al., 2006a; Massenet et al., 2002; Narayanan et al., 2002; Will and Luhrmann, 2001). The steady state level of each snRNA is determined by the gene copy number of that snRNA and by many other factors, including its rate of transcription, processing, transport, assembly, modifications and turnover, as well as availability of both the common and snRNA-specific proteins. Many of these factors could be regulated differently in different cell types and at various stages of development. It is also possible that the SMN complex, in addition to its direct function in Sm core assembly, also plays a role in other steps of snRNP biogenesis and snRNA metabolism. Little is known about the regulation of the

biogenesis and turnover of snRNPs in different tissues, and it will be of interest to study these processes under both normal and SMN deficient conditions.

The splicing changes we observe are widespread, affecting hundreds of genes in different tissues of SMN-deficient mice. Different splicing changes occur in different tissues, but the same splicing changes are observed independently in the same tissue in each of the individual SMN-deficient mice. The very high confirmation rate of changes identified by the exon array and the validation of numerous specific cases by RT-PCR, attest to the high reliability of the data set we obtained. Using the stringent criteria we applied to selection of the affected transcripts, only a fraction of genes for which robust signals were obtained showed splicing perturbations (< 2% of genes). However, the number of affected transcripts is likely to be much higher, because the signals for any given exon represent the average for all transcripts in the tissue. To be detected, a significant change in the signal of an exon would have to occur in a large fraction of the transcripts that contain it. Thus, an aberrant splicing of an exon could be severe in some or even all of the transcripts that contain it in a specific cell population and may not be detectable in the total tissue sample. It is possible that a specific splicing defect that is detrimental to motor neurons occurs but was not detected in the total RNA sample from spinal cord. The lack of an effect on the level of the majority of the transcripts nevertheless indicates that general Pol II transcription and mRNA turnover have not been significantly affected, consistent with cDNA expression microarray experiments using different SMA mouse models with milder phenotypes (Balabanian et al., 2007; Olaso et al., 2006). In many cases, the aberrant splicing generates an mRNA that contains a premature termination codon. These transcripts are present only at very low levels probably because they were subject to nonsense-mediated decay.

Importantly, although some of the changes we observe in specific exons may correspond to shifts in alternative splicing patterns, most of them are not; they are abnormal RNA processing events that give rise to aberrant splicing products, which normally are not produced. We conclude this because many of the exons that are significantly changed in the SMA mice, particularly exon skipping events, are not involved in known alternative splicing events, such as Hif3a (Figure 6), Col5a1 and Uaca (Figure S6). In addition, it is not possible to distinguish based on the available data whether all copies of an affected transcript where more than one exon is aberrantly spliced have the same defect or whether the defects are distributed among many different transcripts.

The mechanistic basis for the widespread splicing defects caused by changes in the levels of SMN, hitherto known to function in the biogenesis of snRNPs, remains to be determined. Splicing is dependent both on snRNPs and RNA-binding proteins (hnRNPs and SR proteins). Knockdowns of mRNA processing factors, including spliceosomal protein components, have been shown to have differential effects on the splicing of a subset of pre-mRNAs in yeast (Clark et al., 2002; Pleiss et al., 2007) and on alternative splicing of a few pre-mRNAs in Drosophila (Park et al., 2004). Rather than depletion of an individual splicing factor, deficiency in SMN, which is not itself a component of the splicing machinery, causes changes in multiple snRNAs, leading to an altered snRNP repertoire. Despite this, there is no reason to believe that the composition of snRNPs within each spliceosome is altered in SMN-deficient cells. Importantly, while changes in the stoichiometry of snRNPs have not been previously associated with global regulation or defects in splicing, our observations merit consideration of such a link. Like the major spliceosomal snRNPs, many of the hnRNP and SR proteins that play a role in splicing are extremely abundant and present in vast excess over their high-affinity binding sites on pre-mRNAs (Dreyfuss et al., 2002; Dreyfuss et al., 1993), yet even moderate changes in their relative stoichiometry have significant effects on alternative splicing patterns (Black, 2003; Hou et al., 2002; Kashima and Manley, 2003; Licatalosi and Darnell, 2006; Martinez-Contreras et al., 2006; Paradis et al., 2007; Wang and Manley, 1995; Zhu et al.,

2001). The complexity of the network of interactions among the snRNPs and between snRNPs and the enormous assortment of splicing factors precludes meaningful prediction of specific splicing outcomes based on a particular snRNA repertoire, at this time. However, we suggest that a change in the stoichiometry of snRNPs perturbs this network and affects the efficiency, rate and fidelity of spliceosome assembly on different introns. Because each cell type has a unique assortment of splicing factors and SMN deficiency causes its snRNP repertoire to change in a unique way, the resulting perturbations are distinct and give rise to cell-type specific effects on splicing. We note, however, that alternative mechanisms cannot be ruled out. For example, the SMN complex could have an snRNA-independent effect on splicing, as experiments with an SMN mutant *in vitro* have suggested (Pellizzoni et al., 1998), or in other aspects of RNA metabolism. Another possible snRNA-dependent scenario for the splicing perturbations is that some unassembled snRNAs accumulate in SMN-deficient cells, which might then sequester snRNP proteins or other proteins required for splicing. The important conclusion nevertheless remains, that the stoichiometry of the major constituents of the splicing machinery (the “snRNPertoire”) is altered and that transcripts reflecting a faulty splicing process accumulate in SMN-deficient cells.

Further studies will be required to uncover the specific mechanism at fault for particular transcripts out of the hundreds or thousands that are affected. The splicing changes we observe in SMN deficiency appear to reflect a general defect in splicing and do not resemble the splicing changes that result from modulation of specific splicing factors (Black, 2003; Caceres et al., 1994; Licatalosi and Darnell, 2006; Ule et al., 2005; Wang and Manley, 1995). However, examination of the affected transcripts reveals several striking features. Pre-mRNAs containing a large number of introns are much more likely to suffer aberrant splicing, suggesting that the likelihood of splicing defects increases with the number of splicing events the transcript undergoes. We note, in addition, that a considerable number of the aberrantly spliced transcripts have more than one splicing abnormality (see Table 1). This appears to exceed the probability of random events and suggests that the affected transcripts have a specific susceptibility to the suboptimal splicing machinery in SMN-deficient cells and that a splicing defect in one intron may be propagated to other introns in the same transcript. We suggest that having a large number of introns makes a transcript more vulnerable to splicing defects upon decreased SMN complex activity, presenting a challenge to evolutionarily more advanced organisms possessing many multi-intron genes. Classification of the aberrantly spliced transcripts by gene ontology indicates that proteins of diverse functions are affected, and reveals a very high preponderance of membrane transporters and extracellular matrix proteins (Table 1). Further analysis of the affected transcripts will be required to determine if there are sequence motifs common to these RNAs that cause their splicing defects. Nevertheless, it is apparent that many of the affected transcripts contain a large number of introns which likely explain their susceptibility.

A new view of SMA emerges from these findings. The selective degeneration of motor neurons is a characteristic feature of SMA, and several potential explanations for this pathogenesis have been suggested, including the possibility of a specific function for SMN in these cells (Monani, 2005). However, our findings that SMN deficiency causes cell type-specific perturbations in the composition of the major components of the spliceosome and a defective transcriptome throughout all cells and tissues, not only motor neurons, indicate that SMA is a general splicing disease. An unanticipated alternative explanation for the motor-neuron selective phenotype in SMA may therefore be that cell-specific factors that influence the relative abundance of individual snRNPs, rather than a cell-specific function of SMN itself, account for the cell-specific phenotype, but their effect is manifested only when SMN, the common factor in the general pathway, becomes limiting. The attrition of motor neurons may be caused by one or more aberrant transcripts or by the cumulative effect of many splicing defects. However, it now seems possible, that splicing defects in surrounding cells, such as those that make up the

matrix on which motor neurons depend, may be the cause or a contributing factor to the demise of the motor neurons. As the severity of SMA is directly correlated with the degree of SMN deficiency, it is likely that even moderate reductions in SMN levels alter the snRNP repertoire and perturb splicing, albeit more subtly than those we have studied here. Together, the observations we describe here establish a key role for the SMN complex in gene regulation, particularly in the maintenance of splicing machinery.

Experimental Procedures

Mouse tissues harvesting

All experiments with mice were carried out in accordance with the NIH Guide for the Care and Use of Laboratory Animals and were approved by the Institutional Animal Care and Use Committee (IACUC Protocol # 800714). The mice were anesthetized with isoflurane and then sacrificed at the indicated age by cervical dislocation. Tissues were collected by manual dissection and either used immediately or frozen in liquid nitrogen and stored at −80°C until further processing.

Reverse transcription and real-time PCR measurement of snRNAs

Total RNA was extracted from culture cells and tissues using mirVana miRNA isolation kit (Ambion). 5S, 5.8S rRNA, and snRNA-specific primers were used to generate cDNA using Advantage RT-for-PCR kit (Clontech). 100 ng (or 375 ng for minor snRNAs) of total RNA was utilized as template in a 20 μl reaction. 1% of the cDNA was used for each real-time PCR reaction.

Real-time PCR experiments for snRNA quantification were carried out on an Applied Biosystems 7500 fast real-time PCR system using SYBR Green I dye chemistry. The same reverse primers were used in both RT and real-time PCR. Each snRNA from mouse tissue or cell samples was measured in triplicates. Absolute quantification was performed using ABI 7500 Fast System Detection Software. Details of all primers and probes are in Table S3.

Exon microarray target preparation, array hybridization, and data analysis

Biotinylated sense-strand DNA targets were prepared using the Affymetrix GeneChip Whole Transcript (WT) Sense Target Labeling Assay according to the manufacturer's directions. 1μg of total RNA from normal (n=3) and SMA (n=3) mouse spinal cord, brain and kidney was used as input for the first round of amplification. 10 μg of the resulting cRNA was used to proceed to the second round of amplification. A hybridization cocktail including 5.5 μg of fragmented, end-labeled ssDNA was applied to GeneChip Mouse Exon 1.0 ST arrays. Hybridization was performed using F450–001 fluidics wash and stain script on the Affymetrix GeneChip Fluidics Station 450. Arrays were scanned using the Affymetrix GCS 3000 7G and GeneChip Operating Software (GCOS) to produce .CEL intensity files.

Probeset intensities were calculated from the CEL files of the 18 samples using the RMA algorithm with default settings at both the gene level and the probeset level in Partek Genomic Suite 6.3, using the core probe sets as defined by Affymetrix. Probesets with maximum RMA intensity of 3 across all samples were excluded to eliminate probesets with low expression levels. Alternative splicing multi-way ANOVA was applied using Partek defaults with terms (probeset ID and group) reflecting not only experimental conditions but also terms that allow detection of alternative splicing events that differ between the sample groups. FDR was calculated and genes with FDR < 0.1 for differential expression or alternative splicing were considered. ANOVA was also applied at the exon level to determine differential expression of exons not grouped by transcript. Functional annotation was performed using DAVID 2007 (http://david.abcc.ncifcrf.gov/home.jsp). The data were analyzed comparing the proportions

of genes with altered splicing against the total genes expressed above background on the microarray.

The exon array data can be accessed at NCBI Gene Expression Omnibus repository (accession number GSE10599).

HT RT-PCR

HT RT-PCR, capillary electrophoresis, and data analysis were performed as previously described (Klinck et al., 2008). PCR primer locations, sequences and electrophoregrams of all reactions are available at http://palace.lgfus.ca/login, using dreyfuss_public and public for username and password, respectively, or upon request from the authors at http://www.med.upenn.edu/dreyfusslab.

Supplementary Material

Refer to Web version on PubMed Central for supplementary material.

Acknowledgements

We are grateful to Drs. Roscoe Klinck and Philippe Thibault for expert and generous help with the HT RT-PCR, Dr. Gordon Lutz for providing the SMA mice, Dr. John Tobias for technical support on exon array data analysis and Drs. Luigi Naldini and Giuliana Ferrari for the pRRL.SIN vector. We thank Isabela Oliva and Quynh Nguyen for technical assistance and the members of our laboratory for stimulating discussions and comments on this manuscript. This work was supported by the Association Française Contre les Myopathies (AFM). G.D. is an Investigator of the Howard Hughes Medical Institute.

References

Baccon J, Pellizzoni L, Rappsilber J, Mann M, Dreyfuss G. Identification and characterization of Gemin7, a novel component of the survival of motor neuron complex. J Biol Chem 2002;277:31957–31962.

Balabanian S, Gendron NH, MacKenzie AE. Histologic and transcriptional assessment of a mild SMA model. Neurol Res 2007;29:413–424. [PubMed: 17535551]

Battle DJ, Kasim M, Yong J, Lotti F, Lau CK, Mouaikel J, Zhang Z, Han K, Wan L, Dreyfuss G. The SMN complex: an assembly machine for RNPs. Cold Spring Harb Symp Quant Biol 2006a;71:313–320. [PubMed: 17381311]

Battle DJ, Lau CK, Wan L, Deng H, Lotti F, Dreyfuss G. The Gemin5 protein of the SMN complex identifies snRNAs. Mol Cell 2006b;23:273–279.

Black DL. Mechanisms of alternative pre-messenger RNA splicing. Annu Rev Biochem 2003;72:291–336. [PubMed: 12626338]

Caceres JF, Stamm S, Helfman DM, Krainer AR. Regulation of alternative splicing in vivo by overexpression of antagonistic splicing factors. Science 1994;265:1706–1709. [PubMed: 8085156]

Carissimi C, Saieva L, Baccon J, Chiarella P, Maiolica A, Sawyer A, Rappsilber J, Pellizzoni L. Gemin8 is a novel component of the survival motor neuron complex and functions in small nuclear ribonucleoprotein assembly. J Biol Chem 2006;281:8126–8134. [PubMed: 16434402]

Charroux B, Pellizzoni L, Perkinson RA, Shevchenko A, Mann M, Dreyfuss G. Gemin3: A novel DEAD box protein that interacts with SMN, the spinal muscular atrophy gene product, and is a component of gems. J Cell Biol 1999;147:1181–1194. [PubMed: 10601333]

Charroux B, Pellizzoni L, Perkinson RA, Yong J, Shevchenko A, Mann M, Dreyfuss G. Gemin4. A novel component of the SMN complex that is found in both gems and nucleoli. J Cell Biol 2000;148:1177–1186. [PubMed: 10725331]

Cifuentes-Diaz C, Frugier T, Melki J. Spinal muscular atrophy. Semin Pediatr Neurol 2002;9:145–150.

Clark TA, Sugnet CW, Ares M Jr. Genomewide analysis of mRNA processing in yeast using splicing-specific microarrays. Science 2002;296:907–910. [PubMed: 11988574]

Dreyfuss G, Kim VN, Kataoka N. Messenger-RNA-binding proteins and the messages they carry. Nat Rev Mol Cell Biol 2002;3:195–205. [PubMed: 11994740]

Dreyfuss G, Matunis MJ, Pinol-Roma S, Burd CG. hnRNP proteins and the biogenesis of mRNA. Annu Rev Biochem 1993;62:289–321. [PubMed: 8352591]

Feng W, Gubitz AK, Wan L, Battle DJ, Dostie J, Golembe TJ, Dreyfuss G. Gemins modulate the expression and activity of the SMN complex. Hum Mol Genet 2005;14:1605–1611. [PubMed: 15843395]

Fischer U, Liu Q, Dreyfuss G. The SMN-SIP1 complex has an essential role in spliceosomal snRNP biogenesis. Cell 1997;90:1023–1029. [PubMed: 9323130]

Gabanella F, Butchbach ME, Saieva L, Carissimi C, Burghes AH, Pellizzoni L. Ribonucleoprotein Assembly Defects Correlate with Spinal Muscular Atrophy Severity and Preferentially Affect a Subset of Spliceosomal snRNPs. PLoS ONE 2007;2:e921. [PubMed: 17895963]

Gabanella F, Carissimi C, Usiello A, Pellizzoni L. The activity of the spinal muscular atrophy protein is regulated during development and cellular differentiation. Hum Mol Genet 2005;14:3629–3642. [PubMed: 16236758]

Gubitz AK, Mourelatos Z, Abel L, Rappsilber J, Mann M, Dreyfuss G. Gemin5, a novel WD repeat protein component of the SMN complex that binds Sm proteins. J Biol Chem 2002;277:5631–5636. [PubMed: 11714716]

Hou VC, Lersch R, Gee SL, Ponthier JL, Lo AJ, Wu M, Turck CW, Koury M, Krainer AR, Mayeda A, et al. Decrease in hnRNP A/B expression during erythropoiesis mediates a pre-mRNA splicing switch. EMBO J 2002;21:6195–6204. [PubMed: 12426391]

Iannaccone ST, Smith SA, Simard LR. Spinal muscular atrophy. Curr Neurol Neurosci Rep 2004;4:74–80. [PubMed: 14683633]

Jablonka S, Wiese S, Sendtner M. Axonal defects in mouse models of motoneuron disease. J Neurobiol 2004;58:272–286.

Kambach C, Walke S, Young R, Avis JM, de la Fortelle E, Raker VA, Luhrmann R, Li J, Nagai K. Crystal structures of two Sm protein complexes and their implications for the assembly of the spliceosomal snRNPs. Cell 1999;96:375–387.

Kashima T, Manley JL. A negative element in SMN2 exon 7 inhibits splicing in spinal muscular atrophy. Nat Genet 2003;34:460–463.

Klinck R, Bramard A, Inkel L, Dufresne-Martin G, Gervais-Bird J, Madden R, Paquet ER, Koh C, Venables JP, Prinos P, et al. Multiple alternative splicing markers for ovarian cancer. Cancer Res 2008;68:657–663. [PubMed: 18245464]

Le TT, Pham LT, Butchbach ME, Zhang HL, Monani UR, Coovert DD, Gavrilina TO, Xing L, Bassell GJ, Burghes AH. SMNDelta7, the major product of the centromeric survival motor neuron (SMN2) gene, extends survival in mice with spinal muscular atrophy and associates with full-length SMN. Hum Mol Genet 2005;14:845–857. [PubMed: 15703193]

Lefebvre S, Burglen L, Reboullet S, Clermont O, Burlet P, Viollet L, Benichou B, Cruaud C, Millasseau P, Zeviani M, et al. Identification and characterization of a spinal muscular atrophy-determining gene. Cell 1995;80:155–165. [PubMed: 7813012]

Licatalosi DD, Darnell RB. Splicing regulation in neurologic disease. Neuron 2006;52:93–101. [PubMed: 17015229]

Liu Q, Fischer U, Wang F, Dreyfuss G. The spinal muscular atrophy disease gene product, SMN, and its associated protein SIP1 are in a complex with spliceosomal snRNP proteins. Cell 1997;90:1013–1021. [PubMed: 9323129]

Lorson CL, Hahnen E, Androphy EJ, Wirth B. A single nucleotide in the SMN gene regulates splicing and is responsible for spinal muscular atrophy. Proc Natl Acad Sci U S A 1999;96:6307–6311. [PubMed: 10339583]

Martinez-Contreras R, Fisette JF, Nasim FU, Madden R, Cordeau M, Chabot B. Intronic binding sites for hnRNP A/B and hnRNP F/H proteins stimulate pre-mRNA splicing. PLoS Biol 2006;4:e21. [PubMed: 16396608]

Massenet S, Pellizzoni L, Paushkin S, Mattaj IW, Dreyfuss G. The SMN complex is associated with snRNPs throughout their cytoplasmic assembly pathway. Mol Cell Biol 2002;22:6533–6541. [PubMed: 12192051]

Meister G, Buhler D, Pillai R, Lottspeich F, Fischer U. A multiprotein complex mediates the ATP-dependent assembly of spliceosomal U snRNPs. Nat Cell Biol 2001;3:945–949. [PubMed: 11715014]

Monani UR. Spinal muscular atrophy: a deficiency in a ubiquitous protein; a motor neuron-specific disease. Neuron 2005;48:885–896. [PubMed: 16364894]

Narayanan U, Ospina JK, Frey MR, Hebert MD, Matera AG. SMN, the spinal muscular atrophy protein, forms a pre-import snRNP complex with snurportin1 and importin beta. Hum Mol Genet 2002;11:1785–1795. [PubMed: 12095920]

Nilsen TW. The spliceosome: the most complex macromolecular machine in the cell? Bioessays 2003;25:1147–1149. [PubMed: 14635248]

Olaso R, Joshi V, Fernandez J, Roblot N, Courageot S, Bonnefont JP, Melki J. Activation of RNA metabolism-related genes in mouse but not human tissues deficient in SMN. Physiol Genomics 2006;24:97–104. [PubMed: 16118268]

Pagliardini S, Giavazzi A, Setola V, Lizier C, Di Luca M, DeBiasi S, Battaglia G. Subcellular localization and axonal transport of the survival motor neuron (SMN) protein in the developing rat spinal cord. Hum Mol Genet 2000;9:47–56. [PubMed: 10587577]

Paradis C, Cloutier P, Shkreta L, Toutant J, Klarskov K, Chabot B. hnRNP I/PTB can antagonize the splicing repressor activity of SRp30c. RNA 2007;13:1287–1300. [PubMed: 17548433]

Park JW, Parisky K, Celotto AM, Reenan RA, Graveley BR. Identification of alternative splicing regulators by RNA interference in Drosophila. Proc Natl Acad Sci U S A 2004;101:15974–15979. [PubMed: 15492211]

Paushkin S, Gubitz AK, Massenet S, Dreyfuss G. The SMN complex, an assemblyosome of ribonucleoproteins. Curr Opin Cell Biol 2002;14:305–312. [PubMed: 12067652]

Pellizzoni L, Baccon J, Charroux B, Dreyfuss G. The survival of motor neurons (SMN) protein interacts with the snoRNP proteins fibrillarin and GAR1. Curr Biol 2001a;11:1079–1088. [PubMed: 11509230]

Pellizzoni L, Baccon J, Rappsilber J, Mann M, Dreyfuss G. Purification of native survival of motor neurons complexes and identification of Gemin6 as a novel component. J Biol Chem 2002a; 277:7540–7545.

Pellizzoni L, Charroux B, Rappsilber J, Mann M, Dreyfuss G. A functional interaction between the survival motor neuron complex and RNA polymerase II. J Cell Biol 2001b;152:75–85.

Pellizzoni L, Kataoka N, Charroux B, Dreyfuss G. A novel function for SMN, the spinal muscular atrophy disease gene product, in pre-mRNA splicing. Cell 1998;95:615–624. [PubMed: 9845364]

Pellizzoni L, Yong J, Dreyfuss G. Essential role for the SMN complex in the specificity of snRNP assembly. Science 2002b;298:1775–1779. [PubMed: 12459587]

Pleiss JA, Whitworth GB, Bergkessel M, Guthrie C. Transcript specificity in yeast pre-mRNA splicing revealed by mutations in core spliceosomal components. PLoS Biol 2007;5:e90. [PubMed: 17388687]

Rossoll W, Jablonka S, Andreassi C, Kroning AK, Karle K, Monani UR, Sendtner M. Smn, the spinal muscular atrophy-determining gene product, modulates axon growth and localization of beta-actin mRNA in growth cones of motoneurons. J Cell Biol 2003;163:801–812. [PubMed: 14623865]

Sauterer RA, Feeney RJ, Zieve GW. Cytoplasmic assembly of snRNP particles from stored proteins and newly transcribed snRNA's in L929 mouse fibroblasts. Exp Cell Res 1988;176:344–359. [PubMed: 2967772]

Schrank B, Gotz R, Gunnersen JM, Ure JM, Toyka KV, Smith AG, Sendtner M. Inactivation of the survival motor neuron gene, a candidate gene for human spinal muscular atrophy, leads to massive cell death in early mouse embryos. Proc Natl Acad Sci U S A 1997;94:9920–9925. [PubMed: 9275227]

Talbot K, Davies KE. Spinal muscular atrophy. Semin Neurol 2001;21:189–197.

Ule J, Ule A, Spencer J, Williams A, Hu JS, Cline M, Wang H, Clark T, Fraser C, Ruggiu M, et al. Nova regulates brain-specific splicing to shape the synapse. Nat Genet 2005;37:844–852. [PubMed: 16041372]

Wan L, Battle DJ, Yong J, Gubitz AK, Kolb SJ, Wang J, Dreyfuss G. The survival of motor neurons protein determines the capacity for snRNP assembly: biochemical deficiency in spinal muscular atrophy. Mol Cell Biol 2005;25:5543–5551. [PubMed: 15964810]

Wang J, Dreyfuss G. A cell system with targeted disruption of the SMN gene: functional conservation of the SMN protein and dependence of Gemin2 on SMN. J Biol Chem 2001;276:9599–9605. [PubMed: 11121410]

Wang J, Manley JL. Overexpression of the SR proteins ASF/SF2 and SC35 influences alternative splicing in vivo in diverse ways. RNA 1995;1:335–346. [PubMed: 7489505]

Waterston RH, Lindblad-Toh K, Birney E, Rogers J, Abril JF, Agarwal P, Agarwala R, Ainscough R, Alexandersson M, An P, et al. Initial sequencing and comparative analysis of the mouse genome. Nature 2002;420:520–562. [PubMed: 12466850]

Whitehead SE, Jones KW, Zhang X, Cheng X, Terns RM, Terns MP. Determinants of the interaction of the spinal muscular atrophy disease protein SMN with the dimethylarginine-modified box H/ACA small nucleolar ribonucleoprotein GAR1. J Biol Chem 2002;277:48087–48093. [PubMed: 12244096]

Will CL, Luhrmann R. Spliceosomal UsnRNP biogenesis, structure and function. Curr Opin Cell Biol 2001;13:290–301. [PubMed: 11343899]

Winkler C, Eggert C, Gradl D, Meister G, Giegerich M, Wedlich D, Laggerbauer B, Fischer U. Reduced U snRNP assembly causes motor axon degeneration in an animal model for spinal muscular atrophy. Genes Dev 2005;19:2320–2330. [PubMed: 16204184]

Yong J, Wan L, Dreyfuss G. Why do cells need an assembly machine for RNA-protein complexes? Trends Cell Biol 2004;14:226–232. [PubMed: 15130578]

Zhang HL, Pan F, Hong D, Shenoy SM, Singer RH, Bassell GJ. Active transport of the survival motor neuron protein and the role of exon-7 in cytoplasmic localization. J Neurosci 2003;23:6627–6637. [PubMed: 12878704]

Zhu J, Mayeda A, Krainer AR. Exon identity established through differential antagonism between exonic splicing silencer-bound hnRNP A1 and enhancer-bound SR proteins. Mol Cell 2001;8:1351–1361. [PubMed: 11779509]

Zieve GW, Sauterer RA, Feeney RJ. Newly synthesized small nuclear RNAs appear transiently in the cytoplasm. J Mol Biol 1988;199:259–267. [PubMed: 3351925]

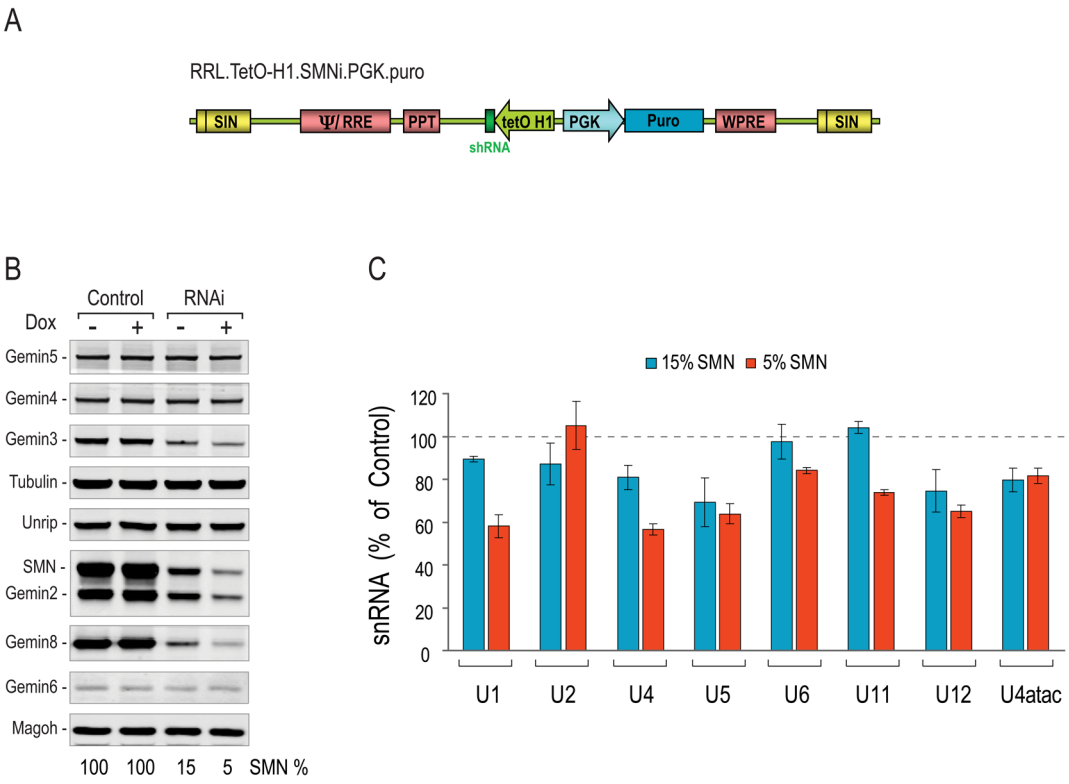

Figure 1. Severe reduction of SMN in HeLa cells causes a strong decrease in snRNPs

(A) Schematic representation of the RRL.TetO-H1.SMNi.PGK.puro lentiviral vector in its proviral form. The U3 region is deleted in both LTRs (SIN, self inactivating; Y, packaging signal; RRE, REV responsive element; PPT, central poly-purine tract; tetO-H1, tetracycline inducible H1 promoter; PGK, phosphoglycerol kinase promoter; Puro, puromycin resistance gene; WPRE, woodchuck hepatitis virus post-transcriptional regulatory element).

(B) Total protein extracts were prepared from HeLa T-REx cells stably expressing shRNAs against mouse SMN (Control) or human SMN (RNAi) without (−) or with (+) doxycycline. SMN complex components were detected by quantitative Western blot, using α-tubulin and Magoh as loading controls.

(C)Total RNA was isolated from Control and RNAi HeLa T-REx cells without (15% SMN, blue columns) or with (5% SMN, red columns) doxycycline. snRNA levels were quantitated by real-time RT-PCR. The snRNA levels of the SMN RNAi cells are plotted as % of control. Same RNAi and snRNA quantitation experiments were done at least three times and one typical experiment was shown. 5S and 5.8S rRNAs levels were used to normalize the RNA input and produced very similar results, therefore only 5S rRNA-normalized data are presented here and in all subsequent real-time RT-PCR measurements for snRNA. The error bars are propagated between SMN and control RNAi samples using the formula:

$$\delta(x/y)/(x/y)=\sqrt{(\delta x/x)^2+(\delta y/y)^2}$$ (δ: SD; *x*: SMA; *y*: Cont).

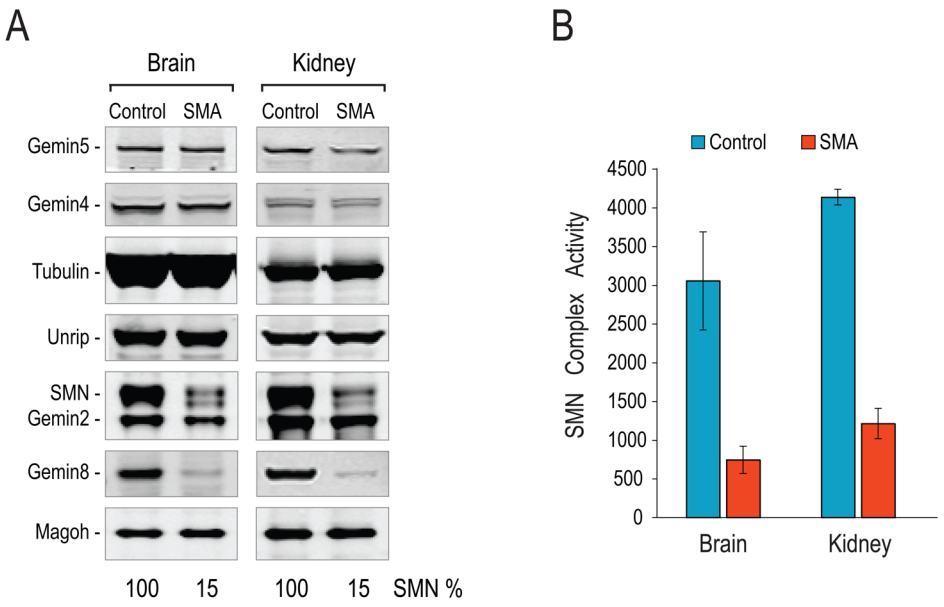

Figure 2. A decrease in SMN complex proteins results in diminished snRNP assembly capacity in SMA mice

(A) Total protein extracts were prepared from brain and kidney of P6 control and SMA mice. SMN and Gemin proteins were detected by quantitative Western blot, using α-tubulin and Magoh as loading controls.

(B) Total protein extracts were prepared as in (A) from P6 control (n=2) and SMA (n=3) mice and snRNP assembly capacities were examined with biotinylated U4 snRNA. Data are presented after subtraction of the background signal relative to U4 ΔSm snRNA. SMN complex activities from various SMA extracts (red columns) were quantitated in comparison to control extract (blue columns). Error bars indicate SD.

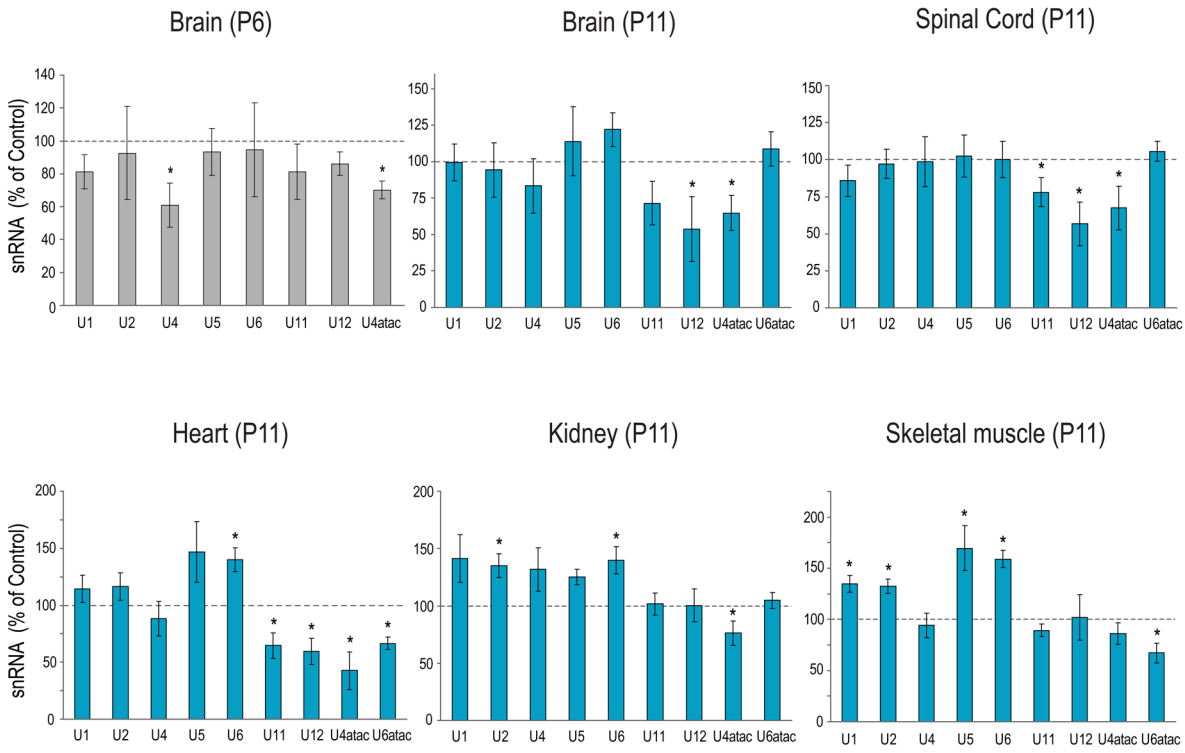

Figure 3. A decrease in SMN complex proteins results in tissue- and snRNP-specific reduction of snRNAs in SMA mice

Total RNA was purified from brain of P6 control (n=2) and SMA (n=3) mice, and brain, spinal cord, heart, skeletal muscle, and kidney of P11 control (n=4) and SMA (n=3) mice. Real-time RT-PCR was performed to determine snRNA levels in each tissue. The relative amount of each snRNA in SMA mice tissues was plotted as % of the controls. Error bars were calculated as in Figure 1C (*P <0.01).

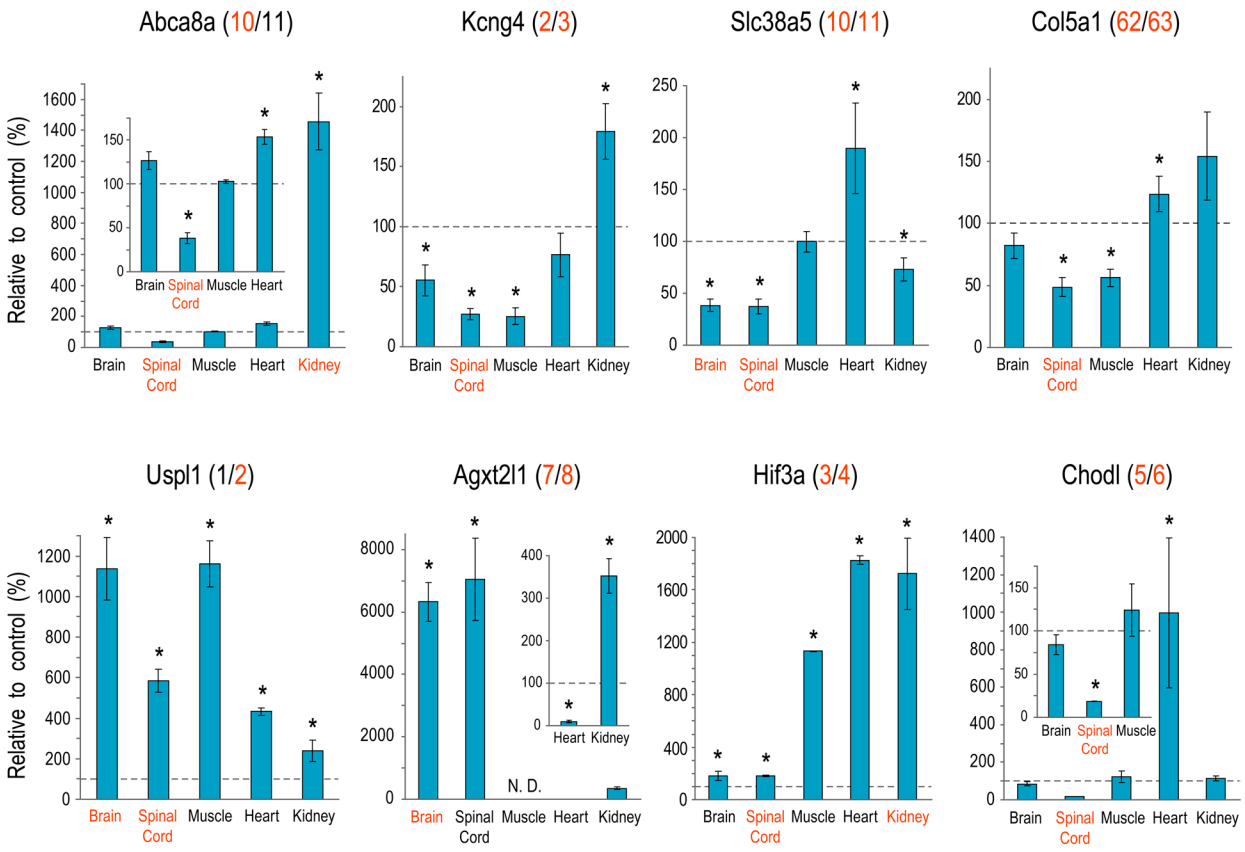

Figure 4. Confirmation of predicted changes in exon expression levels

Exon junction-specific primer/probe sets (indicated in parenthesis after the gene name) were used to measure affected exons from eight genes by real-time RT-PCR, using total RNA prepared from brain, spinal cord, muscle, heart, and kidney tissues of control (n=4) and SMA (n=3) mice. Total RNA inputs were normalized by Gapdh mRNA levels. Exon levels of SMA samples were plotted as % of controls. The affected exons and tissues predicted by exon arrays are highlighted in red. Error bars were calculated as in Figure 1C (* $P < 0.05$).

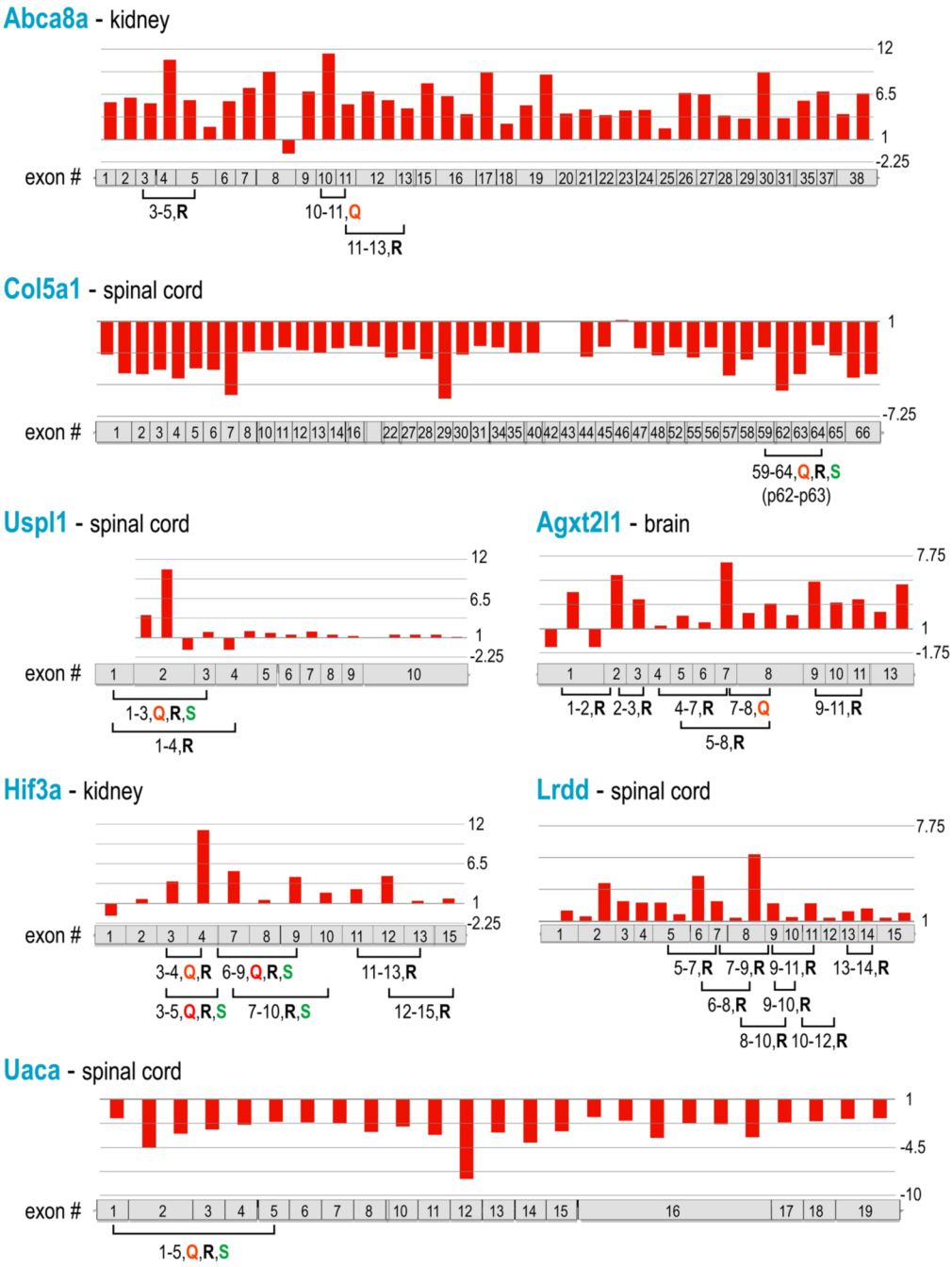

Figure 5. Summary of exon array data and validation for representative genes

Fold-changes of probe sets detecting exon levels (SMA vs. control) are shown on top of the corresponding exon of each gene structure. Note some exons are measured by multiple probesets, while some do not have any targeting probe sets and are not shown in the gene structure. RT-PCR (R), real-time RT-PCR (Q), and sequencing (S) validation reactions are indicated below the gene structure.

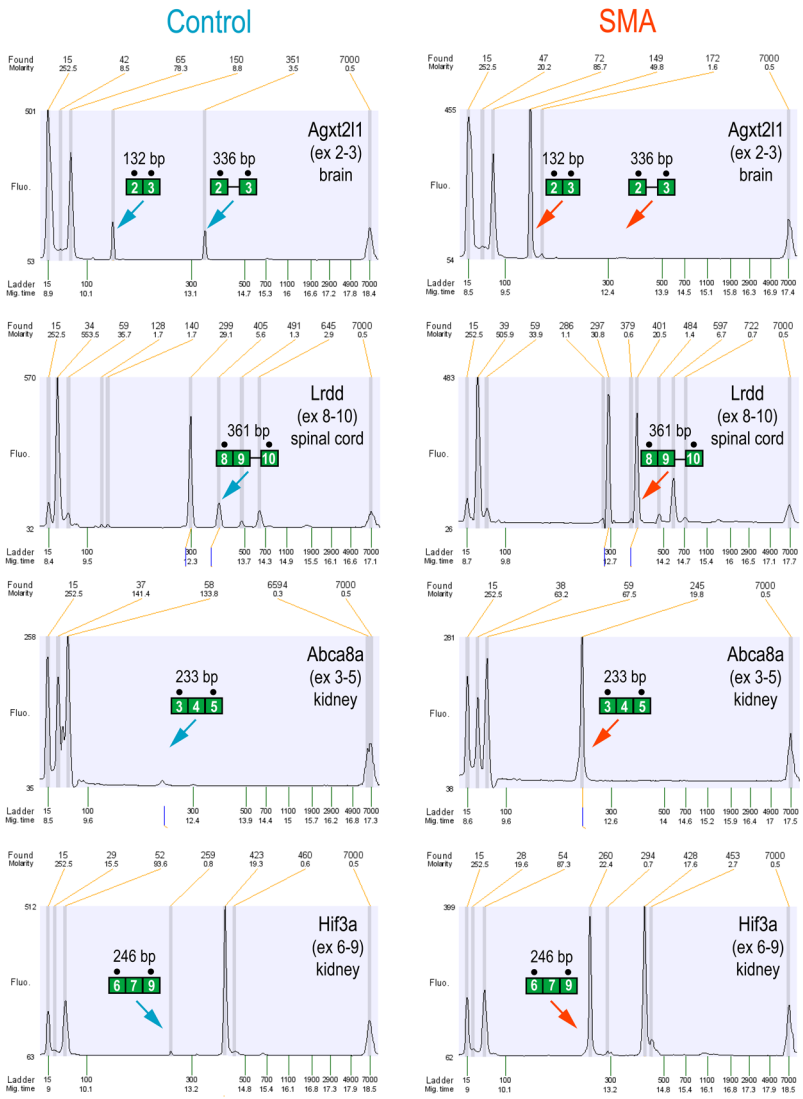

Figure 6. Confirmation of expression and splicing pattern changes by HT RT-PCR reactions

HT RT-PCR reactions characterizing expression and splicing pattern changes of four genes are shown as electrophoregrams. Sizes and molarities of RT-PCR products are listed above the electrophoregrams, and the sizes and migrating times of markers can be found below. Blue and red arrows indicate PCR products representing splicing pattern changes in control and SMA mice, respectively. Relevant PCR products (peaks) were also illustrated by schematic gene structures with predicted sizes. Solid black circles above the exon structures represent primer binding regions.

Table 1

Top 30 genes with one or more exons affected in SMA mice.

Spinal cord							
Accession number	**Gene symbol // Description**	**Biological process or molecular function**	**Fold change of the most affected exon**	**Fold change at transcript level**	**Total affected exons (≥ 1.5 fold)**	**Total exons**	**Validation & Characterization**
NM_183187	BC055107 // cDNA sequence BC055107		17.08	6.82	4	4	Q
NM_009928	Col15a1 // procollagen, type XV	structural molecule activity (extracellular matrix)	−12.67	−3.52	15	40	Q
NM_001013378	Uspl1 // ubiquitin specific peptidase like 1	ubiquitin-dependent protein catabolic process	10.61	1.68	1	10	Q*, R & S
NM_009930	Col3a1 // procollagen, type III, alpha 1	structural molecule activity (extracellular matrix)	−10.59	−3.13	28	51	Q
NM_010220	Fkbp5 // FK506 binding protein 5	protein folding	9.96	4.30	9	10	Q
NM_009864	Cdh1 // cadherin 1	cell adhesion	−8.50	−2.34	7	16	
NM_008608	Mmp14 // matrix metallopeptidase 14 (membrane-inserted)	peptidoglycan metabolic process (extracellular matrix)	−8.50	−2.62	7	10	
NM_028283	Uaca // uveal autoantigen with coiled-coil domains and ankyrin repeats	DNA damage response, signal transduction	−8.10	−2.22	7	19	Q, R* & S
NM_010729	Loxl1 // lysyl oxidase-like 1	protein modification process	−7.94	−2.40	4	7	R
NM_181277	Col14a1 // procollagen, type XIV, alpha 1	structural molecule activity (extracellular matrix)	−7.93	−2.74	18	48	R
NM_139134	Chodl // chondrolectin	muscle development	−7.93	−5.00	6	6	Q*
NM_015784	Postn // periostin, osteoblast specific factor	cell adhesion (extracellular matrix)	−7.84	−2.53	6	22	R
NM_145150	Prc1 // protein regulator of cytokinesis 1	Cytokinesis	−7.68	−2.09	3	14	R
NM_172479	Slc38a5 // solute carrier family 38, member 5	Transport	−7.60	−2.96	9	16	Q & R*
NM_029947	Prdm8 // PR domain containing 8	Transcription	7.09	1.21	1	4	
NM_153145	Abca8a // ATP-binding cassette, sub-family A (ABC1), member 8a	Transport	−7.07	−2.68	15	38	Q & R*
NM_172791	Pla2g3 // phospholipase A2, group III	phospholipid metabolic process	6.87	2.47	3	7	
NM_008489	Lbp // lipopolysaccharide binding protein	transport	−6.81	−2.23	4	15	
NM_007585	Anxa2 // annexin A2	angiogenesis	−6.79	−2.52	10	13	
NM_016868	Hif3a // hypoxia inducible factor 3, alpha subunit	response to hypoxia	6.71	2.09	2	15	Q*, R & S

Spinal cord

Accession number	Gene symbol // Description	Biological process or molecular function	Fold change of the most affected exon	Fold change at transcript level	Total affected exons (≥ 1.5 fold)	Total exons	Validation & Characterization
NM_025734	Kcng4 // potassium voltage-gated channel, subfamily G, member 4	transport	−6.71	−2.34	3	3	Q*
NM_026043	Rnpc3 // RNA-binding region (RNP1, RRM) containing 3	RNA splicing	6.51	1.67	1	15	
NM_172617	Zfp523 // zinc finger protein 523	transcription	−6.23	−1.68	3	15	
NM_172498	Ptk2b // PTK2 protein tyrosine kinase 2 beta	protein amino acid phosphorylation	6.21	1.69	6	30	
NM_007730	Col12a1 // procollagen, type XII, alpha 1	structural molecule activity (extracellular matrix)	−6.17	−2.29	30	66	
NM_007669	Cdkn1a // cyclin-dependent kinase inhibitor 1A (P21)	regulation of progression through cell cycle	6.11	3.20	2	3	
NM_013691	Thbs3 // thrombospondin 3	cell adhesion	5.83	1.48	3	23	
NM_022654	Lrdd // leucine-rich and death domain containing	apoptosis	5.73	1.96	7	15	R
NM_015734	Col5a1 // procollagen, type V, alpha 1	structural molecule activity (extracellular matrix)	−5.70	−1.99	10	66	Q*, R* & S
NM_007742	Col1a1 // procollagen, type I, alpha 1	structural molecule activity (extracellular matrix)	−5.55	−3.07	22	51	Q

Brain

Accession number	Gene symbol // Description	Biological process or molecular function	Fold change of the most affected exon	Fold change at transcript level	Total affected exons (≥ 1.5 fold)	Total exons	Validation & Characterization
NM_030675	Krit1 // KRIT1, ankyrin repeat containing	signal transduction	−12.19	−1.26	1	17	N.D.
NM_011420	Smn1 // survival motor neuron 1	spliceosome assembly	−9.89	−3.43	4	9	
NM_027907	Agxt2l1 // alanine-glyoxylate aminotransferase 2-like 1	metabolism	7.17	2.84	5	13	Q & R**
NM_011623	Top2a // topoisomerase (DNA) II alpha	DNA metabolic process	−7.15	−2.62	6	36	Q
NM_139206	Centd3 // centaurin, delta 3	signal transduction	−5.33	−1.31	2	32	Q
NM_009791	Aspm // asp (abnormal spindle)-like,	cell cycle	−5.07	−1.58	2	28	Q

Spinal cord

Accession number	Gene symbol // Description	Biological process or molecular function	Fold change of the most affected exon	Fold change at transcript level	Total affected exons (≥ 1.5 fold)	Total exons	Validation & Characterization
	microcephaly associated (Drosophila)						
NM_001013	Uspl1 // ubiquitin specific peptidase like 1	ubiquitin-dependent protein catabolic process	4.82	1.48	2	10	Q* & R* & S
NM_001013	Ttf2 // transcription termination factor, RNA polymerase II	transcription	−4.23	−1.17	2	23	
NM_172479	Slc38a5 // solute carrier family 38, member 5	transport	−4.10	−2.01	5	16	Q*
NM_172379	AA536717 // expressed sequence AA536717		−3.96	−1.08	1	7	
NM_011360	Sgce // sarcoglycan, epsilon	cell-matrix adhesion	3.94	1.19	1	11	
NM_009930	Col3a1 // procollagen, type III, alpha 1	structural molecule activity (extracellular matrix)	−3.80	−1.45	3	51	Q
NM_011403	Slc4a1 // solute carrier family 4 (anion exchanger), member 1	transport	−3.80	−1.12	2	20	R
NM_025352	Uqcrq // ubiquinol-cytochrome c reductase, complex III subunit VII	electron transport	3.75	1.34	1	2	
NM_025565	Spc25 // SPC25, NDC80 kinetochore complex component, homolog (S. cerevisiae)	cell cycle	3.60	1.05	1	6	
NM_177049	Jph4 // junctophilin 4	microsome (unknown function)	−3.45	−1.08	1	6	
NM_026539	Chd1l // chromodomain helicase DNA binding protein 1-like	nucleic acid binding	3.10	1.21	1	23	
NM_172274	5730509K17Rik // RIKEN cDNA 5730509K17 gene		3.10	−1.05	1	40	
NM_011984	Homer3 // homer homolog 3 (Drosophila)	protein binding	−2.72	1.18	1	10	
NM_178227	Scn3b // sodium channel, voltage-gated, type III, beta	transport	2.66	1.12	1	5	
NM_026622	3110057O12Rik // RIKEN cDNA 3110057O12 gene		2.58	−1.01	1	12	
NM_146067	C530044N13Rik // RIKEN cDNA C530044N13 gene		2.39	1.27	1	4	
NM_013697	Ttr // transthyretin	thyroid hormone generation	−2.37	−1.08	1	4	
NM_138672	Stab1 // stabilin 1	inflammatory response	−2.30	−1.48	11	69	Q
NM_013869	Tnfrsf19 // tumor necrosis factor receptor superfamily, member 19	apoptosis	2.16	−1.08	2	10	

Spinal cord

Accession number	Gene symbol // Description	Biological process or molecular function	Fold change of the most affected exon	Fold change at transcript level	Total affected exons (≥ 1.5 fold)	Total exons	Validation & Characterization
NM_133817	Zfp451 // zinc finger protein 451	transcription	2.13	1.20	1	15	
NM_177236	Atp2b3 // ATPase, Ca++ transporting, plasma membrane 3	transport	2.12	−1.07	1	21	
NM_021501	Pias4 // protein inhibitor of activated STAT 4	nucleic acid binding	2.06	1.11	1	11	
NM_007730	Col12a1 // procollagen, type XII, alpha 1	structural molecule activity (extracellular matrix)	−2.02	−1.50	2	66	Q
NM_172465	Zdhhc9 // zinc finger, DHHC domain containing 9	zinc ion binding	2.01	−1.12	1	10	

Kidney

Accession number	Gene symbol // Description	Biological process or molecular function	Fold change of the most affected exon	Fold change at transcript level	Total affected exons (≥ 1.5 fold)	Total exons	Validation & Characterization
NM_010009	Cyp27b1 // cytochrome P450, family 27, subfamily b, polypeptide 1	electron transport	54.59	22.25	8	9	Q
NM_010369	Gypa // glycophorin A	cytoskeletal anchoring	−12.61	−3.65	2	8	Q & R
NM_145932	Osta // organic solute transporter alpha	transport	−12.10	−7.21	8	9	
NM_147218	Abca6 // ATP-binding cassette, sub-family A (ABC1), member 6	transport	11.72	3.70	23	39	Q & R
NM_153145	Abca8a // ATP-binding cassette, sub-family A (ABC1), member 8a	transport	11.49	5.31	28	38	Q & R**
NM_016868	Hif3a // hypoxia inducible factor 3, alpha subunit	response to hypoxia	11.20	2.80	7	15	Q*, R* & S
NM_007822	Cyp4a14 // cytochrome P450, family 4, subfamily a, polypeptide 14	electron transport	11.06	4.23	10	12	
NM_011420	Smn1 // survival motor neuron 1	spliceosome assembly	−10.88	−2.85	2	9	
NM_021456	Ces1 // carboxylesterase 1	metabolism	−9.43	−3.58	7	14	

Spinal cord

Accession number	Gene symbol // Description	Biological process or molecular function	Fold change of the most affected exon	Fold change at transcript level	Total affected exons (≥ 1.5 fold)	Total exons	Validation & Characterization
NM_172399	A930038C07Rik // RIKEN cDNA A930038C07 gene		8.85	2.85	4	4	
NM_178259	Abca13 // ATP-binding cassette, sub-family A (ABC1), member 13	transport	8.47	2.91	27	62	Q & R
NM_138595	Gldc // glycine decarboxylase	metabolism	7.93	4.17	24	25	
NM_173767	Insc // inscuteable homolog (Drosophila)	multicellular organismal development	−7.78	−2.33	5	10	
NM_010778	Cd46 // CD46 antigen, complement regulatory protein	single fertilization	7.17	2.26	5	11	Q & R
NM_029939	C330001K17Rik // RIKEN cDNA C330001K17 gene		−7.13	−1.48	2	13	
NM_010220	Fkbp5 // FK506 binding protein 5	protein folding	7.08	4.58	10	10	Q
NM_010061	Dnase1 // deoxyribonuclease I	DNA catabolic process	7.06	3.25	9	9	
NM_181318	Rasgef1b // RasGEF domain family, member 1B	signal transduction	6.83	4.14	14	14	
NM_172466	Adamts18 // a disintegrin-like and metallopeptidase (reprolysin type) with thrombospondin type 1 motif, 18	proteolysis	6.77	1.70	9	23	
NM_008071	Gabrb3 // gamma-aminobutyric acid (GABA-A) receptor, subunit beta 3	transport	−6.44	−3.32	5	10	
NM_025685	Col27a1 // procollagen, type XXVII, alpha 1	structural molecule activity (extracellular matrix)	−6.33	−1.55	9	61	Q
NM_023617	Aox3 // aldehyde oxidase 3	electron transport	6.25	1.57	3	35	
NM_008341	Igfbp1 // insulin-like growth factor binding protein 1	regulation of cell growth	6.24	3.07	2	3	
NM_016771	Sult1d1 // sulfotransferase family 1D, member 1	sulfate assimilation	6.20	3.25	8	8	
NM_021381	Prokr1 // prokineticin receptor 1	signal transduction	−6.17	−2.64	2	3	
NM_029415	Slc10a6 // solute carrier family 10 (sodium/bile	transport	5.97	1.82	4	6	

Spinal cord							
Accession number	**Gene symbol // Description**	**Biological process or molecular function**	**Fold change of the most affected exon**	**Fold change at transcript level**	**Total affected exons (≥ 1.5 fold)**	**Total exons**	**Validation & Characterization**
	acid cotransporter family), member 6						
NM_177200	Svopl // SV2 related protein homolog (rat)-like	transport	5.31	2.52	10	16	
NM_028981	Cacna1d // calcium channel, voltage-dependent, L type, alpha 1D subunit	transport	5.21	1.85	15	48	Q
NM_207216	Ugt3a1 // UDP glycosyltransferases 3 family, polypeptide A1	metabolism	5.02	1.92	5	7	
NM_013454	Abca1 // ATP-binding cassette, sub-family A (ABC1), member 1	transport	5.02	2.41	25	50	

Q: real-time RT-PCR; R: RT-PCR; S: Sequencing; N.D.: Not determined;

* detailed data shown in Figure 4, 5 or 6.